

Animal Study

Potential Molecular Mechanisms of Electroacupuncture With Spatial Learning and Memory Impairment Induced by Chronic Pain on a Rat Model

Jian-Feng Zhang, MD^{1,2}, John P. Williams, MD³, Wan-Rui Shi, MD⁴, Xiao-Yan Qian, CRNA², Qian-Nan Zhao, MD², Guo-Fang Lu, MS², and Jian-Xiong An MD, PhD^{1,2,5}

From: ¹Savaid Medical School, University of Chinese Academy of Sciences, Beijing, China; ²Department of Anesthesiology, Pain and Sleep Medicine, Aviation General Hospital of China Medical University and Beijing Institute of Translational Medicine, Chinese Academy of Sciences, Beijing, China; ³Department of Anesthesiology, University of Pittsburgh School of Medicine, Pittsburgh, PA, USA; ⁴Department of Anesthesiology, Peking University Third Hospital, Beijing, China; ⁵School of Medical Science & Engineering, Beijing Advanced Innovation Center for Biomedical Engineering, Beihang University, Beijing, China

Address Correspondence:
Jian-Xiong An, MD, PhD
Department of Anesthesiology
Pain and Sleep Medicine,
Aviation General Hospital of China
Medical University
Beiyuan Road 3# Beijing 100012
People's Republic of China
E-mail: anjianxiong@yeah.net

Disclaimer: This study was supported by the National Natural Science Foundation of China, Beijing, China. (81671076) and (82072086). All authors report no biomedical financial interests.

Conflict of interest: Each author certifies that he or she, or a member of his or her immediate family, has no commercial association (i.e., consultancies, stock ownership, equity interest, patent/licensing arrangements, etc.) that might pose a conflict of interest in connection with the submitted manuscript.

Manuscript received: 07-23-2021
Revised manuscript received: 09-26-2021

Accepted for publication: 11-09-2021

Free full manuscript: www.painphysicianjournal.com

Background: It is frequently reported that neuropathic pain is associated with abnormalities in brain function and structure as well as cognitive deficits. However, the contributing mechanisms have remained elusive.

Objectives: We aimed to investigate the systemic ultrastructural changes of the peripheral nervous system (PNS) and central nervous system (CNS) in rats with trigeminal neuralgia (TN) induced by cobra venom, as well as the effects and mechanisms of electroacupuncture (EA) and pregabalin (PGB) on TN.

Study Design: This study used an experimental design in rats.

Setting: The research took place in the laboratory at the Aviation General Hospital of China Medical University and Beijing Institute of Translational Medicine.

Methods: Male Sprague-Dawley rats were randomly divided into 4 groups (n = 12/group): cobra venom (CV), PGB, EA, and sham-operated (SHAM). The development of pain-related behaviors and spatial learning and memory abilities were measured using video recordings and Morris water maze tests, respectively. The ultrastructural changes of the PNS and CNS were examined using transmission electron microscopy. We also screened the differentially expressed genes and proteins in the prefrontal cortex and hippocampus using ribonucleic acid sequencing and isobaric tag for relative and absolute quantitation techniques, respectively. Data for the behavioral tests and molecular biology were analyzed with a one-way analysis of variance.

Results: The rats in the CV group exhibited long-lasting pain-like behaviors, cognitive deficits, and systemic ultrastructural changes. Both EA and PGB alleviated the chronic pain syndrome, but EA also inhibited the chronic pain-induced cognitive dysfunction and restored normal cellular structures, while PGB was associated with no improvements. Transcriptomic and proteomic analyses revealed *marcks*, *pak2* and *acat1* were altered in rats with TN but were adjusted back to baseline by EA but not by PGB.

Limitations: We examined systemic ultrastructural alterations at different levels of the nervous system; however, the detailed timeline of the damage process was not explicitly delineated. Moreover, the current study provides only preliminary evidence for the neurobiological mechanisms of cognitive impairment resulting from chronic pain. Further research is still necessary (using models such as gene knockout rats and cell cultures) before a detailed mechanism can be postulated.

Conclusions: EA treatment may offer significant advantages when compared to PGB for the treatment of cognitive impairment associated with chronic pain. Moreover, *marcks*, *pak2* and *acat1* may be the potential therapeutic targets of EA.

Key words: Trigeminal neuralgia, cognitive dysfunction, electroacupuncture, pregabalin, ultrastructural changes, prefrontal cortex, hippocampus

Pain Physician 2022; 25:E271-E283

Trigeminal neuralgia (TN) is recognized as a chronic pain disorder that has been described as the most severe pain one can experience (1). Patients who suffer from painful conditions typically have alterations in their behavioral and psychological responses (2), such as anxiety disorders, depressive disorders (3), insomnia (4), and alterations in cognitive function (5), all of which have a negative effect on their quality of life. Studies have revealed that chronic TN dramatically changes the functional architecture of the brain including the primary somatosensory cortex, secondary somatosensory cortex, prefrontal cortex (PFC), amygdala, hippocampus, insular cortex, anterior cingulate cortex, thalamus, cerebellum, and periaqueductal gray matter (6). The gray matter volume in several brain areas mentioned above are reduced in patients with chronic pain conditions (7). Additionally, the PFC and hippocampus are most often associated with spatial learning and memory in humans and rodents (8-11). Treatments designed to improve these cognitive alterations are essential for effective management of TN. Electroacupuncture (EA), the combination of acupuncture and electric stimulation, is effective in the treatment of patients not only with chronic pain (12), but also with cognitive dysfunction (13).

In this study, we examined systemic ultrastructural changes in the peripheral nervous system and central nervous system (CNS) in rats with TN induced by cobra venom. Moreover, the effects of EA and pregabalin (PGB) for treating TN were also assessed. In addition, transcriptomics (ribonucleic acid sequencing [RNA-Seq]) and proteomics (isobaric tag for relative and absolute quantitation [iTRAQ]-based) were applied to assess the mechanism of cognitive dysfunction induced by chronic TN as well as the cognitive effects of EA. We also examined the potential targets and molecular signaling pathways associated with EA treatment of chronic TN-induced alterations in spatial learning and memory. In addition, western blot and immunofluorescence were carried out to confirm the expression of proteins. This study will help to elucidate the potential mechanisms of cognitive impairment induced by chronic pain as well as the therapeutic targets for EA stimulation.

METHODS

The entire experimental procedure on conscious animals was approved by the Ethical Committee of Aviation General Hospital of China Medical University and was in accordance with the Guidelines for the Care and

Treatment of Laboratory Animals of the US National Institutes of Health.

Animals

Forty-eight healthy male Sprague-Dawley rats weighting between 200g-260g from the Beijing Vital River Laboratory Animal Technology Co., Ltd Medical Science (Beijing, China) were used in these experiments. The animals were housed 6 per cage and maintained in a 12h/12h light/dark cycle with food and water available ad libitum. All the experiments were performed in accordance with the guidelines set by the Animal Care and Use Committee (Beijing, China). The animals were randomly divided into 4 groups (n = 12/group) by using a random number table: sham-operated (SHAM), cobra venom (CV), EA and PGB.

Surgery Procedure

The procedure has been described in detail by An et al (14). Animals were anesthetized with 1% Pelltobarbitalum Natricum (40 mg/kg body weight intraperitoneally, AMRESCO, Solon, OH). A one-centimeter incision was made along the superciliary arch to expose the fossa orbitalis and nasal bone. The left infraorbital nerve (ION) was freely dissected and raised gently by a glass nerve dissector. Rats in the CV, EA and PGB groups were injected into the nerve sheath of the ION with a mixture of lyophilized CV and isotonic saline (0.1mg/μL; Venom Research Institute of Guangxi Medical University) to a total dose of 4 μL. The SHAM group underwent the same procedure except that 4 μL of saline was injected instead of CV. The incision was closed using 5-0 absorbable sutures.

Electroacupuncture Treatment

According to our previous study (15), from the 14th day to the 35th day after TN modeling, a 30-minute EA treatment was applied once every 2 days in the EA group, as the 14th day after operation is considered the point of transformation from acute to chronic pain (16). Briefly, the acupuncture was applied at the left forelimb at the "Shousanli" (LI10) and "Quchi" (LI11). Then, the rats were treated with EA stimulation using an Acupoint Nerve Stimulator (LH series, Peking University, China). The frequency of EA stimulation was automatic shifting between 2 Hz and 100 Hz (frequency sweeping; pulse width: 0.6 milliseconds in 2 Hz and 0.1 milliseconds in 100 Hz, each lasting for 3 seconds) (17,18). Current intensity was maintained at 1 mA, then increased to 1.5 mA and finally increased to 2 mA; each period lasted 10 minutes.

PGB Administration

For drug treatments, PGB (75 mg; Pfizer, New York, NY) was dissolved in 7.5 mL of sterilized saline and administered intragastrically at a dose of 30 mg/kg once a day, consecutively for 21 days from postoperative day 14 to day 35 (15).

Spontaneous Pain Assessments

The rats were tested on preoperative days 3 and 7, as well as 14, 21, 27, 35 and 40 days postsurgery. Rats were placed in a transparent plastic cage (24 x 35 x 18 cm) with a video camera placed one m in front of the cage with a clean mirrored back (15,19-21). The frequency and length of exploratory activity and grooming were videotaped and analyzed offline by 2 investigators who were blinded as to the treatment group. The less exploratory behavior and the more grooming behavior exhibited, the higher the presumptive degree of pain.

The Morris Water Maze Test

Rats were tested 4 times (preoperative day 7 and 7, 21, and 35 days postsurgery) for spatial learning and memory using a visual platform in a water maze. Briefly, the training trial was performed 4 times per day for 4 days, and the probe trial was carried out at day 5. During the training trial, the length of the path and time taken by the rats to reach the platform was recorded. The average percentage time of the total probe trial time in the target quadrant and the number of exact site crossings were calculated in the probe trial.

Transmission Electron Microscopy

On postoperative day 40, the bilateral PFC, bilateral hippocampus, thalamus, medulla oblongata, the cross section of the spinal cord and bilateral dorsal root ganglion (DRG) (the sectioning and DRG were only obtained for the C7, T12 and L5 sections), bilateral Gasserian ganglion, bilateral ION, thoracic and lumbar cord levels and bilateral brachial plexus, 12th-13th spinal thoracic nerve and sciatic nerves were dissected and immersed in 3% glutaraldehyde for 24 hours, and rinsed with 0.1 M phosphate buffer 3 times. Then the tissues were fixed with osmium tetroxide (Sigma, St. Louis, MO) for 2 hours, and cut into one- μ m plastic sections before being dehydrated and then embedded in araldite for 24 hours. The sections were recorded under a transmission electron microscope (TEM; H-9000NARiBaraki, Hitachi Ltd., Tokyo, Japan)

after staining with uranyl acetate. The investigators were blinded to the experimental groups during reading of TEM images.

PFC and Hippocampus Extraction

Rats were euthanized at 40 days postsurgery and the PFC and hippocampus were quickly removed and dissected free while the brains were placed on ice. These regions were then flash-frozen and kept at -80°C for further transcriptomics and proteomics analysis.

Transcriptomics

Total RNA was extracted from the tissues using Trizol (Invitrogen, Carlsbad, CA). As previous described (22), the library preparation of polyA-enriched RNA from total RNA was performed by Beijing Genomics Institute (BGI, Shenzhen, China). The resultant library was sequenced with BGISEQ500 platform (BGI-Shenzhen, China). Raw data from the sequencing was filtered using the internal software SOAPnuke (<https://github.com/BGI-flexlab/SOAPnuke>) to get clean reads by removing reads containing adapter sequences and low-quality reads. Then clean reads were subjected to novel gene prediction, SNP & INDEL calling and gene-splicing detection after mapping the clean reads onto a reference genome (GCF_000001895.5_Rnor_6.0). The differentially expressed genes were identified between different samples and the clustering analysis and functional annotations were performed.

Proteomics

The samples were detected for iTRAQ-based proteomic analysis at the Beijing Genomics Institute (BGI, Shenzhen, China). According to the methods described previously, the proteomics protocol was conducted based on BGI guidelines. In the present research, proteins of the PFC and hippocampus from the 4 groups were extracted and digested into peptides. The desalted peptides were labeled with iTRAQ reagents (SCIEX, Framingham, MA). The PFC of the SHAM, CV, EA, and PGB groups were labeled with 114, 116, 118, and 121 iTRAQ tags. The hippocampal specimens of the SHAM, CV, EA, and PGB groups were labeled with 113, 115, 117, and 119 iTRAQ tags. The mixed peptides were analyzed by LTQ-Orbitrap-Velos hybrid mass spectrometer (Thermo Fisher Scientific, Inc., Waltham, MA) coupled with liquid chromatography (Thermo Fisher Scientific, Inc.) and strong cation exchange chromatography.

Details of the Morris water maze test, transcriptomics and proteomics are in Supplemental Material 1.

Western Blot

Proteins (30 µg) from samples were boiled in 6×Laemmli loading buffer for 5 minutes, then transferred to 0.2 µm Polyvinylidene-Fluoride membranes (Millipore Corporation, Burlington, MA) after 10% SDS-polyacrylamide gels. Meanwhile, the blots were blocked in blocking solution (5% nonfat dry milk, 0.05% Tween-20 in PBS) at 37°C for 2 hours, then incubated overnight with antisera (dilution): β-actin (1:2000) (Santa Cruz Biotechnology, Inc., Dallas, TX), marcks (1:5,000) (Abcam, Cambridge, UK), pak2 (1:3000) (Abcam, Cambridge, UK), kcna2 (1:200) (Alomone Labs, Jerusalem, Israel), acat1 (1: 500) (Abcam, Cambridge, UK) at 4°C. The blots were visualized via horseradish peroxidase-conjugated goat anti-rabbit secondary antibody (1:20000) (CW0103, Beyotime Institute of Biotechnology, Shanghai, China) and evaluated by performing ECL detection system (Millipore Corporation, Burlington, MA). The bands corresponding to marcks, Pak2, kcna2, acat1, and β-actin were scanned and quantitatively analyzed.

Immunofluorescence

Immunofluorescence staining of target factors was performed. PFC and hippocampus samples from each group were immersed in 4% paraformaldehyde, cryosectioned, and incubated with primary and secondary antibodies. The following antibodies were used as primary antibodies: pak2(1:200), acat1(1:200), and marcks (1:200). The secondary antibodies were as follows: Fluorescein-isothiocyanate-labeled goat anti-mouse IgG (GB22301, dilution ratio 1: 200), Cy3-conjugated goat anti-rabbit IgG (GB21303, dilution ratio 1: 200), and Cy5-conjugated goat anti-rabbit IgG (GB27303, dilution ratio 1: 200). TSA Cyanine 3 system (TSA Plus Fluorescence Kit, PerkinElmer; G1236-100T) was used for immunostaining. Immunofluorescence was detected by Panoramic Scanner (Panoramic DESK, P-MIDI, P250; 3DHISTECH, Budapest, Hungary).

Statistics

Quantitative analysis, statistical comparisons, and data analysis were performed using SPSS Version 23.0 (IBM Corporation, Armonk, NY). Western blots and immunofluorescence are quantified by Image J software (National Institutes of Health, Bethesda, Maryland). Data for the behavioral test and the Morris water maze

test were assessed for normal distribution by the Shapiro—Wilk test and analyzed with one-way analysis of variance and two-way repeated measures of analysis of variance followed by the Tukey test for post hoc comparisons. Results are presented as the mean ± standard deviation. $P < 0.05$ was considered as statistically significant.

RESULTS

General Observations

Five rats in the model group died within 3 days. The penetration of venom into the surrounding tissue of the ION could represent the cause of their deaths. There was no mortality after cobra venom or vehicle injection after postoperative day 3. Moreover, the body weight did not differ among the groups.

Behavioral Changes

There were no significant differences among the 4 groups in exploratory behaviors and grooming behaviors before the operation nor at postoperative day 3. From postoperative day 7, the exploratory behaviors of rats in the CV group were significantly reduced compared to the SHAM group, and the grooming behaviors of rats in the CV group were significantly increased. In the EA and PGB groups, there were no significant differences between groups. However, the 2 groups demonstrated a significant increase in exploratory behavior while grooming behavior showed a significant reduction compared with the CV group at postoperative day 21 until the end of the experiment (Fig. 1).

Changes in Spatial Learning and Memory

In the Morris water maze test, escape latency and the number of exact site crossings were similar in all groups at the preoperative assessment and 7 days postsurgery. At postoperative day 21 and day 35, the time taken by the rats to reach the platform was reduced and the number of platform crossings was increased in the EA group compared with the CV group and PGB group, but showed no significant difference from the SHAM group. Simultaneously, in the PGB group, there were no significant differences when compared to the CV group. However, the rats in the PGB group showed significant increases in escape latency and decreases in the number of exact site crossings compared with the EA group and SHAM group, respectively (Fig. 2).

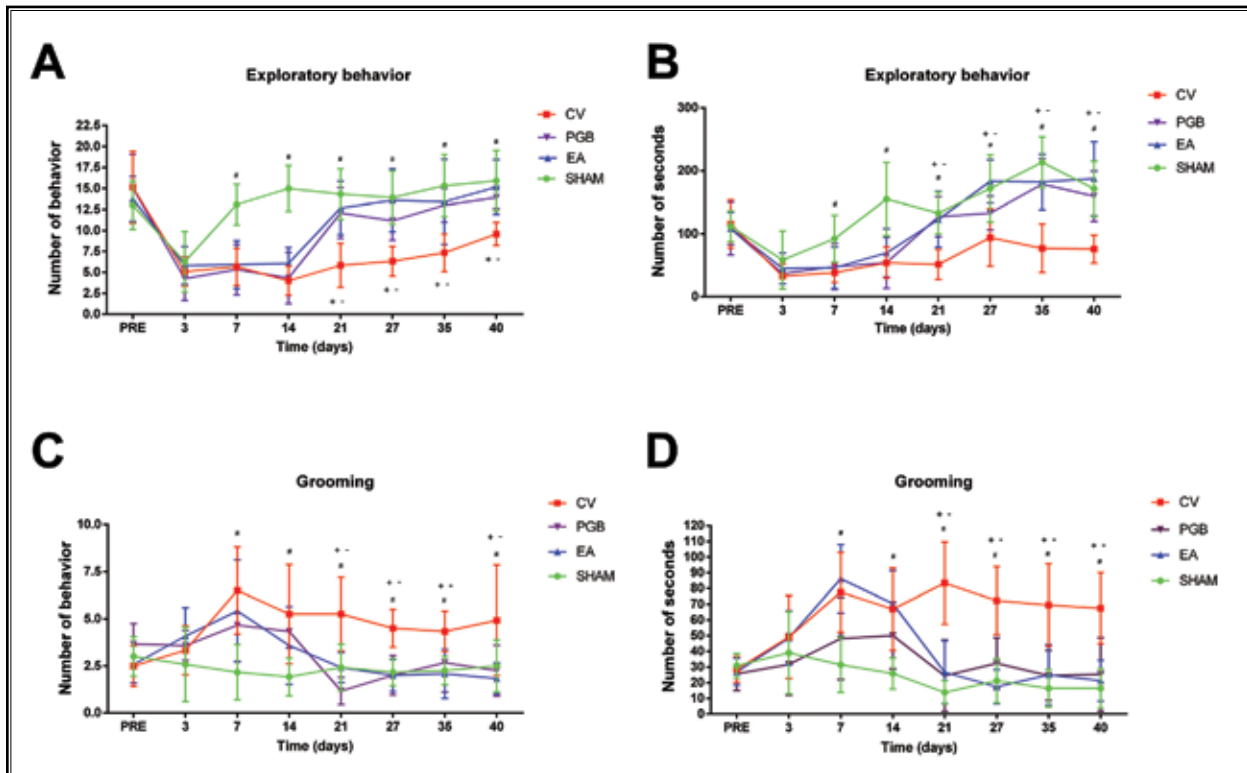


Fig. 1. Frequency and length of observed face-grooming and exploratory behaviors were observed before the operation (pre) and at 7 postoperative time points.

(A) The frequency of exploratory behavior. (B) The length of exploratory behavior. (C) The frequency of face-grooming. (D) The length of face-grooming. No significant baseline differences between groups were found prior to 3 days postoperatively. The rats with TN exhibited spontaneous pain behaviors from day 7 postsurgery compared to the rats in the SHAM group. Moreover, both EA and PGB could alleviate the spontaneous pain in rats with TN from day 21 after surgery. Data are presented as mean \pm standard deviation (SD). #, -, + $P < 0.05$.

SHAM: sham-operated; CV: cobra venom; EA: electroacupuncture; PGB: pregabalin.

Ultrastructure Detected by Transmission Electron Microscopy

In this study, we found that the left ION and Gasserian ganglion, bilateral PFC, hippocampus, thalamus, medulla oblongata, spinal dorsal horn at cervical (C7), thoracic (T12), and lumbar (L5) levels were damaged in the rats with chronic pain. These pathological changes were specifically manifested as follows: destroyed mitochondria and axons, and dissolved surrounding tissues were observed in bilateral PFC and hippocampus. Similarly, moderately severe loss of cristae junctions as well as detachment of cristae membranes from the inner boundary membrane in mitochondria were observed in the thalamus. In addition, the medulla oblongata, cross section of the spinal cord, and left ION and left Gasserian ganglion (operative side) displayed extensive demyelination. However, there were no corresponding ultrastructural changes in the peripheral nervous

system except ipsilateral ION and Gasserian ganglion mentioned above.

We further confirmed a definite ultrastructural change secondary to EA stimulation and PGB. Mild swelling of the myelin sheath was observed in the cross section of the spinal cord, ipsilateral ION and Gasserian ganglion, which was better than that in the CV group. Normal-shaped cells with intact myelin sheaths and axons could be seen on the bilateral PFC, bilateral hippocampus and the thalamus in the EA group. However, the effect was not found in the PGB treatment group. Dissolved myelin sheaths and damaged mitochondria and axons were still visible in these structures. Furthermore, while treatment with EA attenuated demyelination in the medulla oblongata, this was not seen with PGB. The results described above suggest that EA and PGB can restore normal structures at various levels of the spinal cord as well as damaged ION and Gasserian

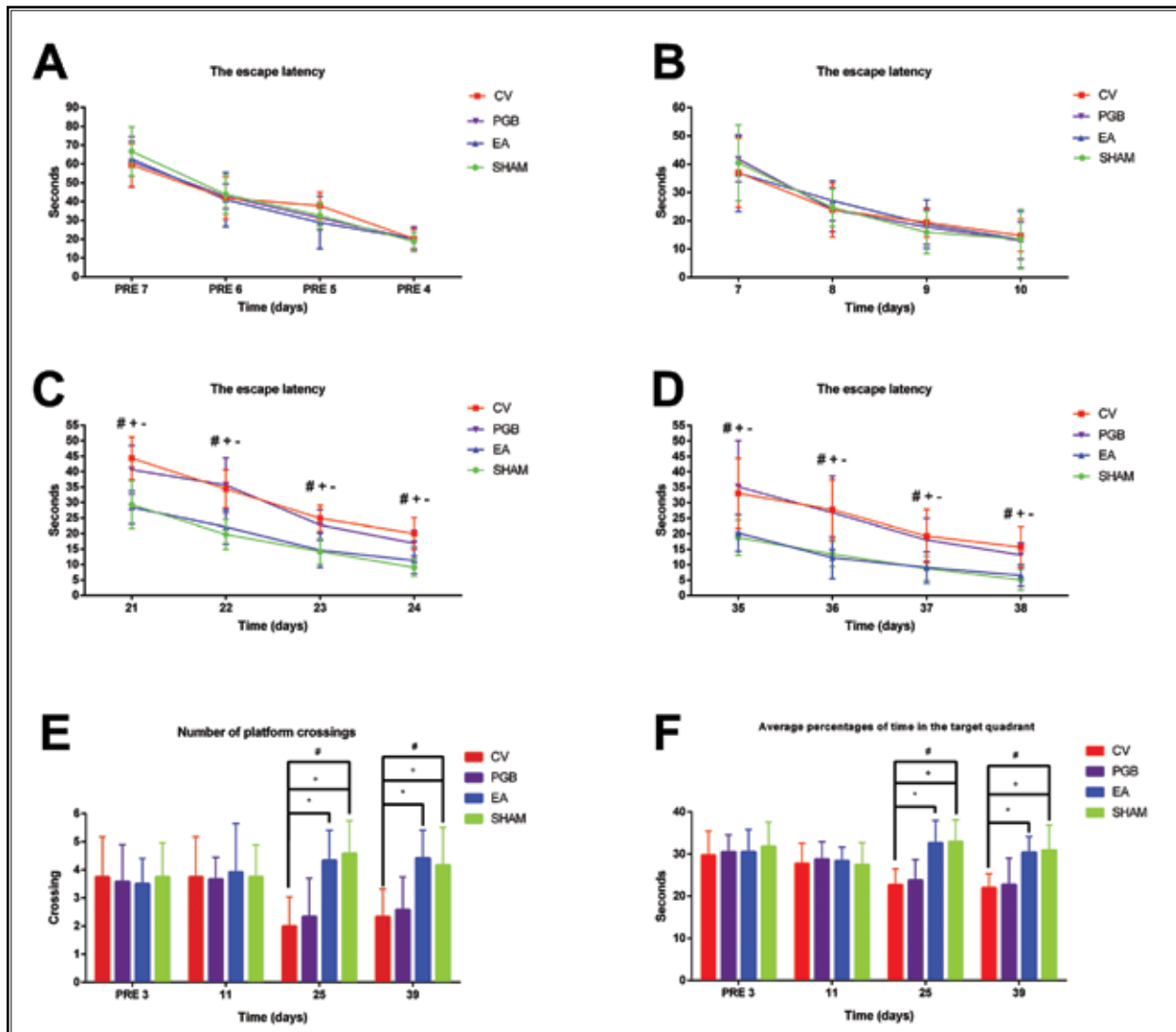


Fig. 2. Behavioral performance of rats in the Morris water maze. (A, B) Morris water maze training trial at preoperative day 7 to 4 and postoperative days 7 to 10, respectively. No differences were observed in the latency curve among all groups. (C, D) Morris water maze training trial at postoperative days 21 to 24, and postoperative days 35 to 38, respectively. Decreased spatial learning abilities were observed in rats with TN (escape latencies were remarkably increased compared with those in the SHAM group). The escape latencies were decreased in the EA group compared with the CV group and PGB group. (E) The number of exact site crossings in the Morris water maze probe training trial at preoperative day 3, postoperative days 11, 25, and 39. (F) Percent time spent in the target quadrant during the probe trials. The number of exact site crossings and percent time spent in the target quadrant were significantly decreased in the CV and PGB groups compared with the SHAM and EA groups at postoperative days 25 and 39. This suggests that the spatial memory abilities in rats with TN were significantly decreased. The rats in the EA group had normal memory abilities. Data are presented as mean \pm SD. #, -, +, * $P < 0.05$. SHAM: sham-operated; CV: cobra venom; EA: electroacupuncture; PGB: pregabalin.

ganglion. Further, EA was also associated with restoration of normal structures in the PFC, hippocampus, thalamus and medulla oblongata, while PGB was associated with no improvement. However, this is a

nonquantitative, observational finding. Figure 3 summarizes the systemic ultrastructural changes. A detailed description of these morphological results is shown in Supplemental Material 2.

Transcriptomic Study

We preliminarily analyzed the PFC among all groups by RNA-Seq. We set the absolute value of log₂ (fold change) ≥ 2 and q-value ≤ 0.001 as filter condition. To detect the effects of EA treatment on cognitive disorders, we also screened out the genes that were significantly changed in the CV group compared to the SHAM group and adjusted back to the baseline by EA stimulation (without PGB treatment) in PFC (Fig. 4A) and hippocampus (Fig. 5A). The detailed gene and protein information can be found in Supplemental Table 1.

In order to detect the mechanism of pain-induced cognitive recovery related to treatment with EA, we screened out the genes that demonstrated a significantly differential gene expression in the CV group compared to the SHAM group and adjusted back to baseline by EA treatment. Interestingly, gene ontology (GO) analysis identified enriched biological processes associated with “positive regulation of cytosolic calcium ion concentration,” “adenylate cyclase-inhibiting serotonin receptor signaling pathway,” “regulation of dopamine secretion,” “regulation of dopamine meta-

bolic process,” and “negative regulation of synaptic transmission, glutamatergic” in the PFC, indicating that EA treatment may improve pain-induced cognitive disorders by regulating neuropeptide signaling pathways associated with serotonin and dopamine levels (Fig. 4B). In the hippocampus, GO analysis showed that these genes were mainly enriched in the telencephalon and organismal development (Fig. 5B).

Proteomic Analysis

In order to better elucidate the mechanisms of cognitive disorders in chronic pain, the PFC and hippocampal samples were also analyzed for overall protein identification by iTRAQ. According to the data from respective replicates, 3,502 proteins were identified. We set the absolute value of log₂ (fold change) ≥ 1.15 and q-value ≤ 0.001 as filter condition. We screened out the proteins that were significantly changed in the CV group compared to the SHAM group and adjusted back to the baseline following EA treatment. There were only 8 proteins meeting the screening requirements in the PFC: LOC301124, nup214, snrnp70, marcks, p2rx4, LOC680875, cntn4, and cript2 (Fig.

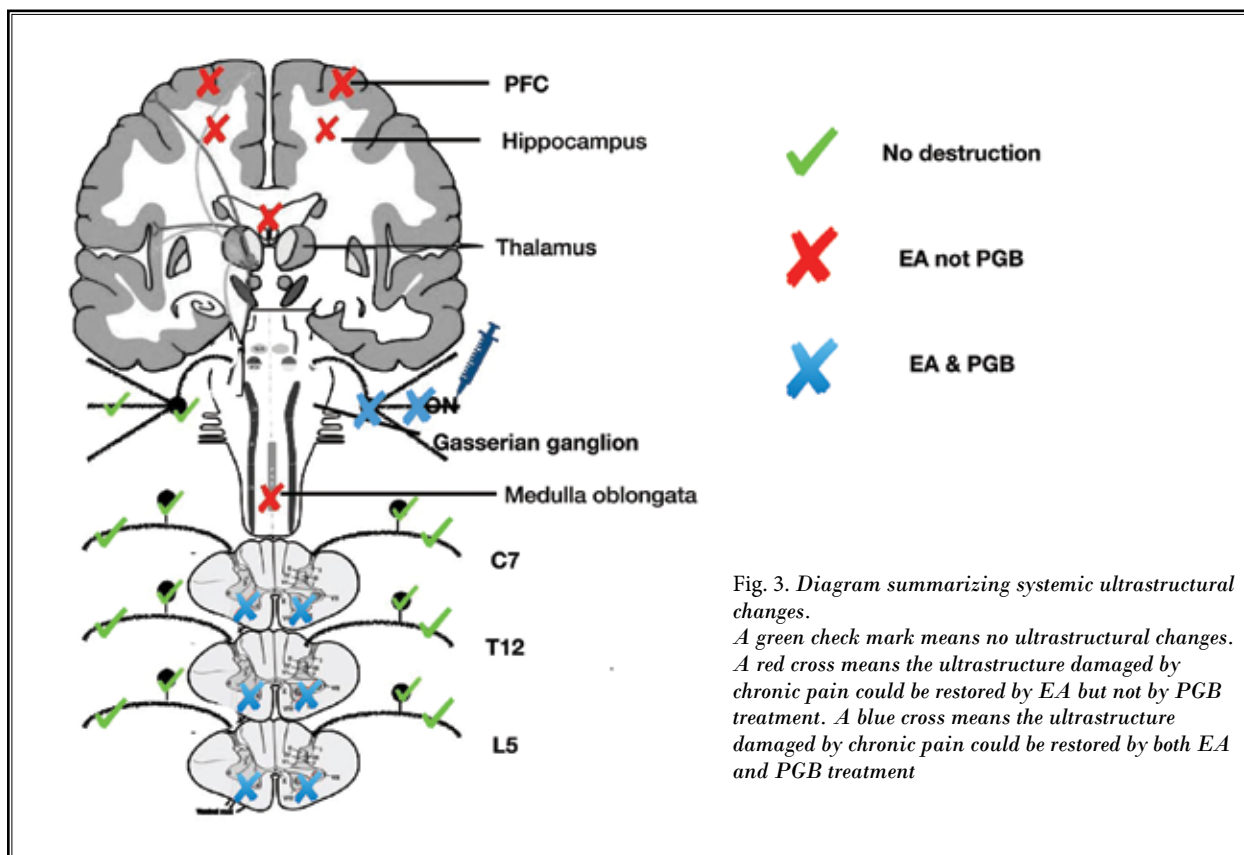


Fig. 3. Diagram summarizing systemic ultrastructural changes. A green check mark means no ultrastructural changes. A red cross means the ultrastructure damaged by chronic pain could be restored by EA but not by PGB treatment. A blue cross means the ultrastructure damaged by chronic pain could be restored by both EA and PGB treatment

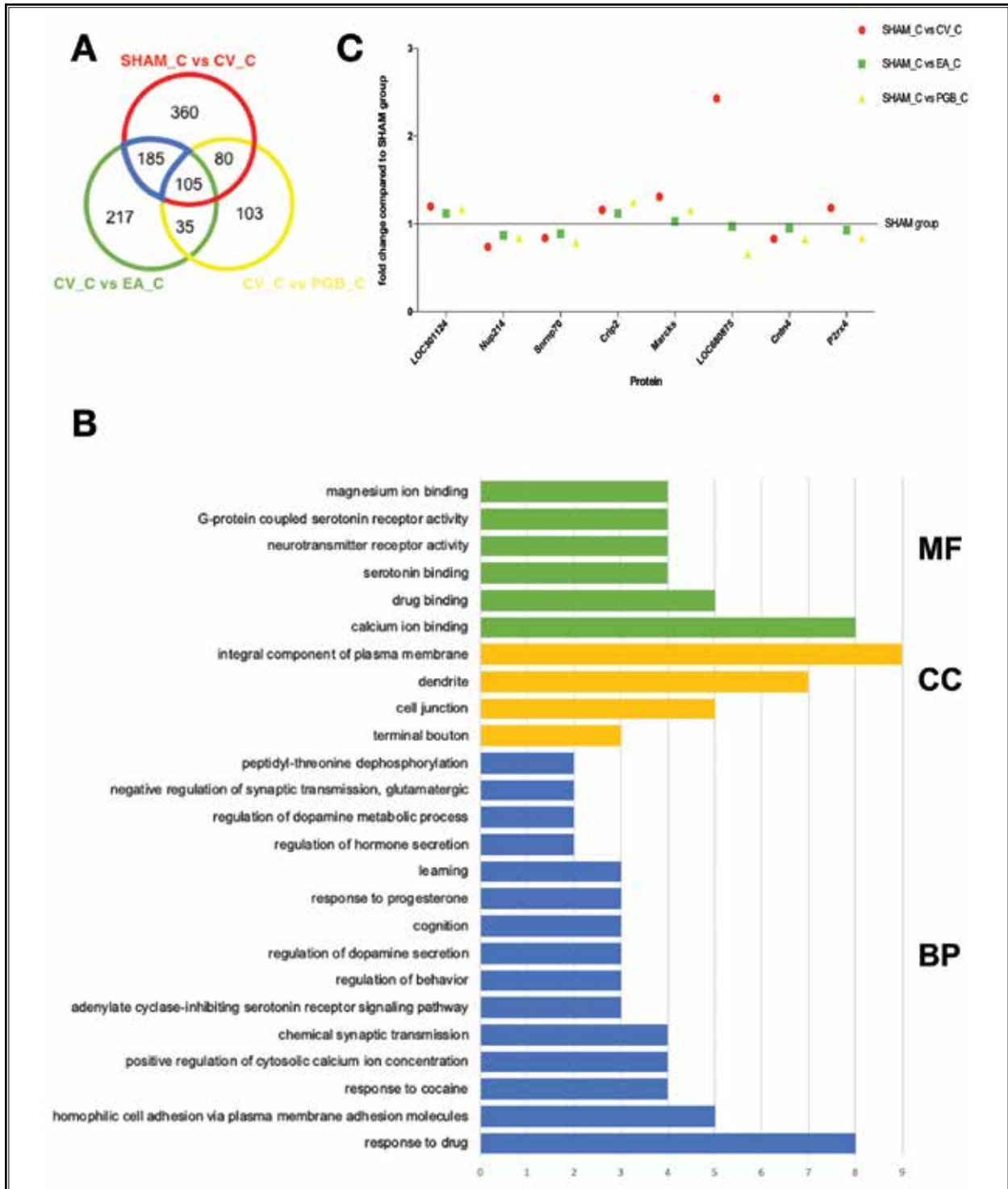


Fig. 4. The data of genomic and proteomic analysis in the PFC.

(A) The special genes screen rules to detect the effects of EA treatment on cognitive disorder in the PFC. The genes in PFC that are significantly changed in the CV group compared to the SHAM group and adjusted back to the baseline by EA treatment (without PGB treatment) were singled out. (B) The GO analysis of 119 genes screened out via special rules in the PFC. (C) The 8 proteins selected by the special screen rules in the PFC.

SHAM: sham-operated; CV: cobra venom; EA: electroacupuncture; PGB: pregabalin; GO: Gene ontology; PFC: prefrontal cortex.

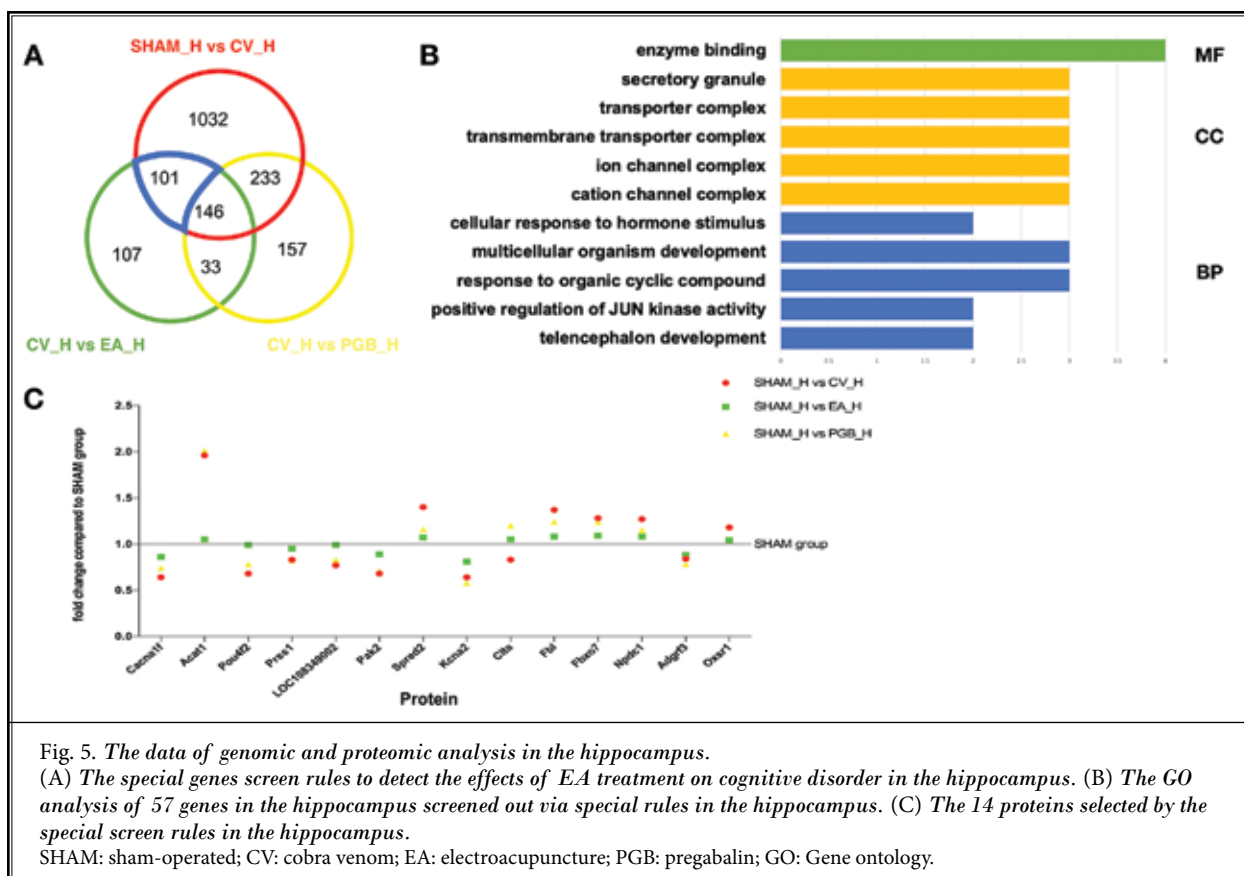


Fig. 5. The data of genomic and proteomic analysis in the hippocampus. (A) The special genes screen rules to detect the effects of EA treatment on cognitive disorder in the hippocampus. (B) The GO analysis of 57 genes in the hippocampus screened out via special rules in the hippocampus. (C) The 14 proteins selected by the special screen rules in the hippocampus. SHAM: sham-operated; CV: cobra venom; EA: electroacupuncture; PGB: pregabalin; GO: Gene ontology.

4C). We also screened out 14 proteins according to the rules mentioned above in the hippocampus, that is, cacna1f, acat1, pou4f2, prss1, LOC108349002, pak2, spred2, kcna2, cta, fbl, fbxo7, npdc1, adgrf3, and oxsr1 (Fig. 5C).

The detailed results of transcriptomic and proteomic analysis are shown in Supplemental Material 3.

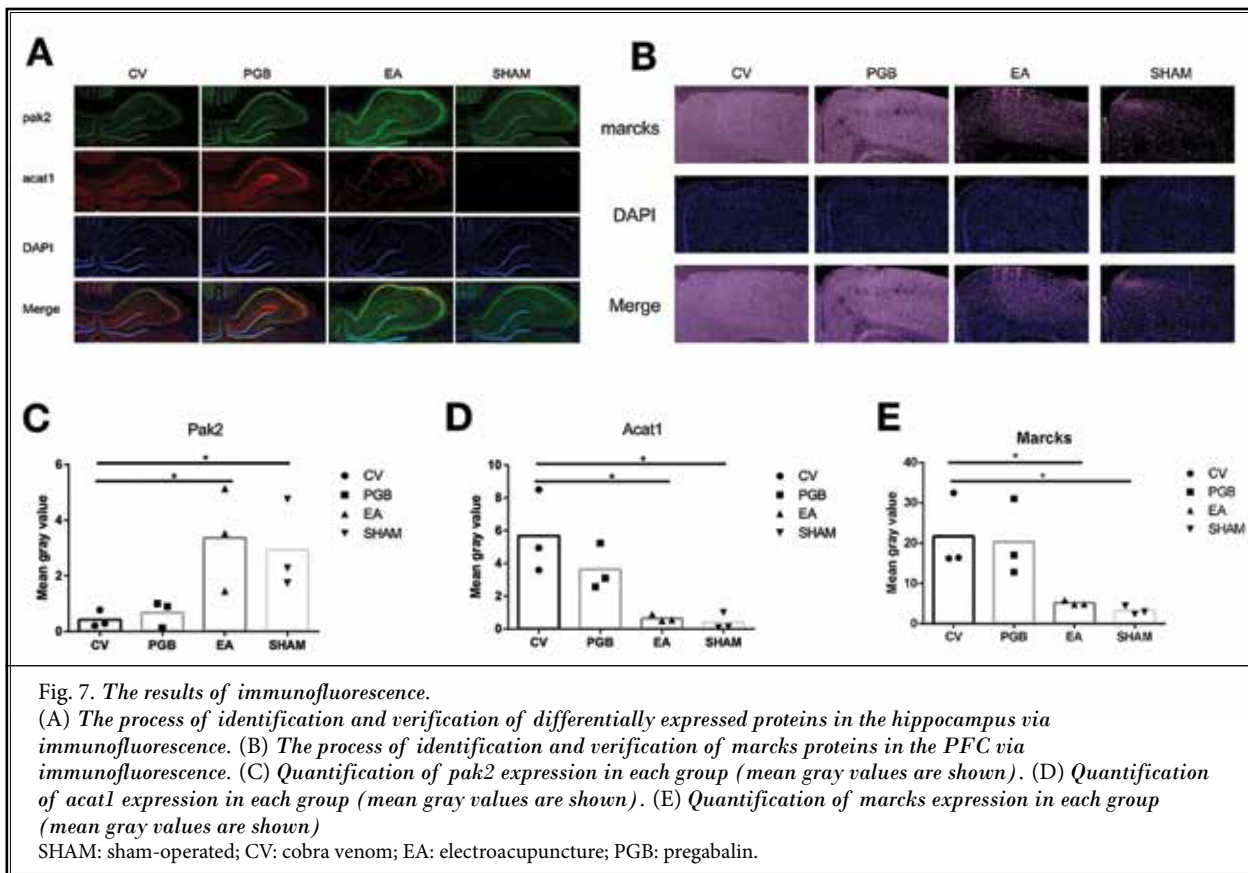
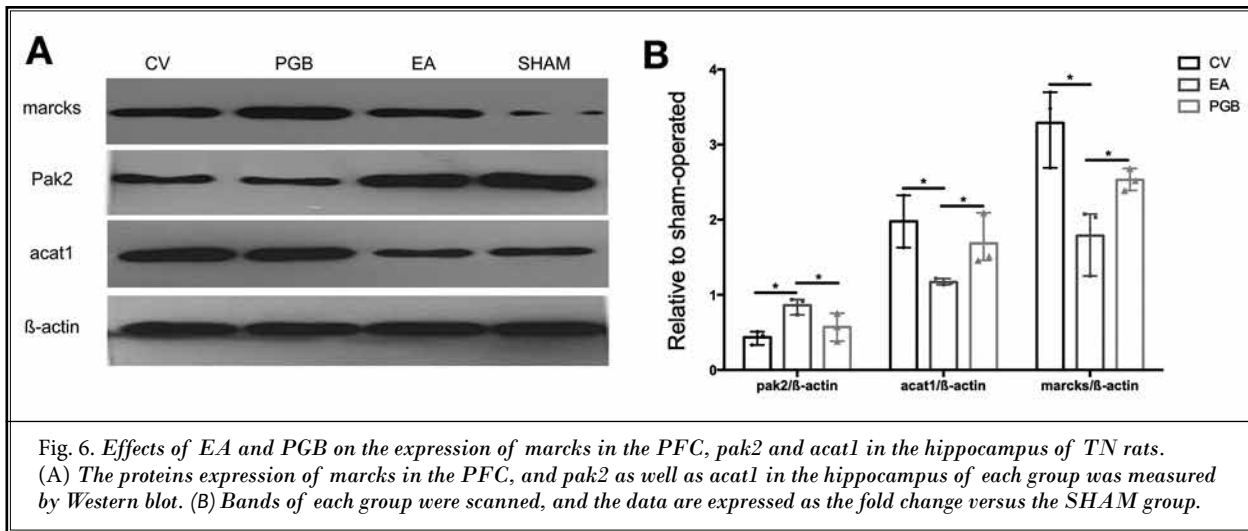
Identification and Verification of Differentially Expressed Proteins

To detect the potential mechanism of cognitive dysfunction induced by chronic pain and the molecular targets of EA treatment in improving cognitive abilities, we compared the genes and proteins screened via special screen rules mentioned above in both transcriptomic and proteomic studies. We found only one protein in the PFC (marcks) and 3 proteins in the hippocampus (pak2, acat1, kcna2) respectively that met our criteria. Furthermore, we measured the protein levels of marcks in the PFC and pak2, acat1, kcna2 in the hippocampus through Western blot. The results showed that the level of marcks in the CV and PGB groups were lower than in the SHAM and EA

groups. There were higher levels of pak2 and acat1 in the CV and PGB groups compared with the SHAM and EA groups in the hippocampus (Fig. 6). There were no significant changes in the level of kcna2 (results not shown). To determine the specificity of these proteins, immunostaining was performed to confirm the proteins' expression among groups. Confocal images of the PFC and the hippocampus showed that the majority of immunofluorescence was surrounded by cytoplasm and that similar protein expression changes were associated with Western blot (Fig. 7).

DISCUSSION

In the present study, we found that the rats with TN exhibited long-lasting pain-like behaviors and cognitive deficits. Both EA and PGB alleviated chronic pain syndrome, but EA also inhibited chronic pain-induced cognitive dysfunction, while PGB was associated with no improvement. This is consistent with our previous results (15,23,24). Currently, many studies have investigated the analgesic efficacies of PGB in several illnesses characterized by neuropathic pain. However, there are



several compelling lines of evidence that suggest that there are also adverse cognitive effects of PGB. Kawano and colleagues (25) demonstrated that PGB could prevent, but not treat, rats with postoperative cognitive dysfunction. Some clinical studies also show that PGB

can induce neurotoxicity complaints and negative cognitive effects in healthy volunteers (26,27). In addition, a 2-part, 4-way crossover study from Okkerse and colleagues (28) showed that somnolence was observed in 31%, nausea in 31%, and dizziness in 56% of the

patients receiving PGB for pain control. Therefore, the data from these studies, as well as our present study, suggest that treatment of neuropathic pain solely with PGB may lead to unsatisfactory outcomes, especially if the pain is accompanied by cognitive impairment.

In contrast, there is compelling research on the role of EA for treating both neuropathic pain as well as cognitive dysfunction. Several lines of evidence support a direct effect of EA on different types of pain, such as chronic low back pain (12,29) and osteoarthritis of the knee (30). However, the evidence of the effects of EA for treating cognitive dysfunction is both sparse and limited in quality; although, there have been several preclinical studies examining the role of EA in illnesses characterized by cognitive impairment (13,31,32). We believe that chronic pain may result in cognitive changes secondary to changes in both brain structure and function.

Systemic ultrastructural changes were observed at different levels of the CNS in rats with TN. Many previous publications have reported that neural damage in the periphery results in changes in both brain activity and central circuits (20,33,34). One possibility is the gliopathy associated with inflammation in the CNS. Several lines of evidence suggest that mechanical allodynia induced by neuropathic pain is a neuroinflammatory response in the CNS that is characterized by aberrant microglial activation in the spinal cord (35,36). Notably, the activation of microglia could play a pathogenic role in ultrastructural alterations such as demyelination or axonal degeneration in CNS (37,38). However, this is speculation on our part.

We confirmed a definite ultrastructural change secondary to EA stimulation and PGB. Similar to the results obtained by Shiers et al (39), our current work suggests that the variable therapeutic effects of EA and PGB on the ultrastructure of the CNS may be associated with the impact of these treatments on cognitive dysfunction.

To determine the potential mechanism of cognitive dysfunction induced by chronic pain as well as the molecular targets of EA treatment in improving cognitive abilities, we examined the transcriptome and proteome of the PFC and hippocampus. We used stringent filters to select a limited number of genes and proteins. One hundred nineteen genes and 8 proteins in the PFC were screened. The only overlap between transcriptome and proteome analyses was marcks. The myristoylated alanine-rich C kinase substrate (marcks) is critical for fundamental processes such as neurite outgrowth, endo and exocytosis, and synaptic plasticity and has emerged as an

essential regulator of the dynamic actin cytoskeleton (40). Overexpression of marcks not only induces significant alterations in the appearance of dendritic protrusions but impairs hippocampal dependent learning and memory (41). The alterations of marcks in the PFC are more related to mental disorders such as schizophrenia and bipolar disorder (42). In the present study, the level of marcks in the PFC increased in the CV group compared to the SHAM group and was adjusted back to normal with EA therapy. This finding led us to hypothesize that the level of marcks plays a key role in persistent pain-induced cognitive impairment, and this protein could be a potential therapeutic target for EA treatment.

We also singled out 57 genes and 14 proteins via special rules in the hippocampus. Two proteins were selected by integrating transcriptomic and proteomic data, which were *acat1* and *pak2*. As a member of the p21-activated protein kinase (*pak*) family, *pak2* is involved in many processes including cell proliferation, apoptosis, mitosis, and angiogenesis. But the significance of the activation of *pak2* in the CNS has not been fully elucidated. Wang et al (43) suggested that a *pak2* deficiency extensively perturbs functional networks associated with autism spectrum disorder. This protein acts by regulating actin cytoskeleton dynamics, resulting in markedly decreased synaptic densities, defective long-term potentiation, and autism-related behaviors in mice (43). Long-term changes in connections between neurons are thought to be the basis of learning and memory formation. Actin cytoskeleton dynamics are integral to both structural and functional synaptic plasticity. Additionally, studies also reported that the level of *pak2* was associated with a variety of neurodevelopmental and neurodegenerative disorders (44,45). Thus, we infer that a potential mechanism of cognitive impairment after chronic pain and the subsequent therapeutic effects of EA are closely related to the level of *pak2* and the stability of the cytoskeleton.

There is one critique and several limitations to this study that we would like to acknowledge. First the critique: that is, widespread damage in the CNS is caused by the distribution of cobra venom by blood circulation. This is highly unlikely as rats with penetration of venom into the surrounding tissue of the ION generally succumb within a few minutes. Now for our limitations: our morphological study is nonquantitative and observational in nature. Further quantitative analysis is the direction for our future work. Secondly, we used very stringent statistical filters (0.1%) and this might have limited the discovery of other associated moieties.

Finally, the current study provides only preliminary evidence for the neurobiological mechanisms of cognitive impairment resulting from chronic pain. The results of this study are based on in vivo experiments and therefore must be verified by using in vitro assays and clinical studies. Further research into this topic is still necessary before a detailed mechanism using such models as gene knockout rats and cell cultures can be applied.

CONCLUSIONS

EA treatment may offer significant advantages when compared to PGB for the treatment of cognitive impairment associated with chronic pain. Moreover, marcks, pak2 and acat1 may be the potential therapeutic targets of EA.

Supplemental materials 1, 2 and 3 can be obtained by contacting the corresponding author.

REFERENCES

- Di Stefano G, Maarbjerg S, Truini A. Trigeminal neuralgia secondary to multiple sclerosis: From the clinical picture to the treatment options. *J Headache Pain* 2019; 20:20.
- Gilam G, Gross JJ, Wager TD, Keefe FJ, Mackey SC. What is the relationship between pain and emotion? Bridging constructs and communities. *Neuron* 2020; 107:17-21.
- Gerrits MM, van Oppen P, Leone SS, van Marwijk HW, van der Horst HE, Penninx BW. Pain, not chronic disease, is associated with the recurrence of depressive and anxiety disorders. *BMC Psychiatry* 2014; 14:187.
- Afolalu EF, Moore C, Ramlee F, Goodchild CE, Tang NK. Development of the Pain-Related Beliefs and Attitudes about Sleep (PBAS) Scale for the assessment and treatment of insomnia comorbid with chronic pain. *J Clin Sleep Med* 2016; 12:1269-1277.
- Meskal I, Rutten GJ, Beute GN, Salden ME, Sitskoorn MM. Cognitive deficits in patients with trigeminal neuralgia: Opportunities to improve care and quality of life. *Acta Neurochir (Wein)* 2014; 156:1565-1566.
- Zhang C, Hu H, Das SK, Y et al. Structural and functional brain abnormalities in trigeminal neuralgia: A systematic review. *J Oral Facial Pain Headache* 2020; 34:222-235.
- Sundermann B, Dehghan Nayyeri M, Pfeleiderer B, et al. Subtle changes of gray matter volume in fibromyalgia reflect chronic musculoskeletal pain rather than disease-specific effects. *Eur J Neurosci* 2019; 50:3958-3967.
- Barron HC, Dolan RJ, Behrens TE. Online evaluation of novel choices by simultaneous representation of multiple memories. *Nat Neurosci* 2013; 16:1492-1498.
- Peters J, Büchel C. Episodic future thinking reduces reward delay discounting through an enhancement of prefrontal-mediocortical interactions. *Neuron* 2010; 66:138-148.
- Spellman T, Rigotti M, Ahmari SE, Fusi S, Gogos JA, Gordon JA. Hippocampal-prefrontal input supports spatial encoding in working memory. *Nature* 2015; 522:309-314.
- Birnbaum SG, Yuan PX, Wang M, et al. Protein kinase C overactivity impairs prefrontal cortical regulation of working memory. *Science* 2004; 306:882-884.
- Kong JT, Puetz C, Tian L, et al. Effect of electroacupuncture vs sham treatment on change in pain severity among adults with chronic low back pain: A randomized clinical trial. *JAMA Netw Open* 2020; 3:e2022787.
- Yang Y, Hu S, Lin H, He J, Tang C. Electroacupuncture at GV24 and bilateral GB13 improves cognitive ability via influences the levels of A β , p-tau (s396) and p-tau (s404) in the hippocampus of Alzheimer's disease model rats. *Neuroreport* 2020; 31:1072-1083.
- An JX, He Y, Qian XY, et al. A new animal model of trigeminal neuralgia produced by administration of cobra venom to the infraorbital nerve in the rat. *Anesth Analg* 2011; 113:652-656.
- Chen RW, Liu H, An JX, et al. Cognitive effects of electro-acupuncture and pregabalin in a trigeminal neuralgia rat model induced by cobra venom. *J Pain Res* 2017; 10:1887-1897.
- Quinn R. Comparing rat's to human's age: how old is my rat in people years? *Nutrition* 2005; 21:775-777.
- Han JS. Acupuncture: neuropeptide release produced by electrical stimulation of different frequencies. *Trends Neurosci* 2003; 26:17-22.
- Hubacher J, Niemtow RC, Corradino MD, JDunn JCY, Ha DH. Standards for reporting electroacupuncture parameters. *Medical Acupuncture* 2016; 28:249-255.
- Vos BP, Strassman AM, Maciewicz RJ. Behavioral evidence of trigeminal neuropathic pain following chronic constriction injury to the rat's infraorbital nerve. *J Neurosci* 1994; 14:2708-2723.
- Wu Z, Qian XY, An JX, et al. Trigeminal neuralgia induced by cobra venom in the rat leads to deficits in abilities of spatial learning and memory. *Pain Physician* 2015; 18:E207-E216.
- An JX, Shi WR, Zhang JF, et al. A new rat model of thalamic pain produced by administration of cobra venom to the unilateral ventral posterolateral nucleus. *Pain Physician* 2019; 22:E635-E647.
- Luo X, Cao D, Li H, et al. Complementary iTRAQ-based proteomic and RNA sequencing-based transcriptomic analyses reveal a complex network regulating pomegranate (*Punica granatum L.*) fruit peel colour. *Sci Rep* 2018; 8:12362.
- Zhao QQ, Qian XY, An JX, et al. Rat model of trigeminal neuralgia using cobra venom mimics the electron microscopy, behavioral, and anticonvulsant drug responses seen in patients. *Pain Physician* 2015; 18:E1083-1090.
- Zhang L, Ding X, Wu Z, Qian X, An J, Tian M. Trigeminal neuralgia induced by cobra venom leads to cognitive deficits associated with downregulation of CREB/BDNF pathway. *Pain Physician* 2017; 20:53-68.
- Kawano T, Eguchi S, Iwata H, et

- al. Pregabalin can prevent, but not treat, cognitive dysfunction following abdominal surgery in aged rats. *Life Sci* 2016; 148:211-219.
26. Salinsky M, Storzbach D, Munoz S. Cognitive effects of pregabalin in healthy volunteers: A double-blind, placebo-controlled trial. *Neurology* 2010; 74:755-761.
 27. Beltramini GC, Cendes F, Yasuda CL. The effects of antiepileptic drugs on cognitive functional magnetic resonance imaging. *Quant Imaging Med Surg* 2015; 5:238-246.
 28. Okkerse P, van Amerongen G, de Kam ML, et al. The use of a battery of pain models to detect analgesic properties of compounds: A two-part four-way crossover study. *Br J Clin Pharmacol* 2017; 83:976-990.
 29. Francescato Torres S, Brandt de Macedo AC, Dias Antunes M, et al. Effects of electroacupuncture frequencies on chronic low back pain in older adults: Triple-blind, 12-months protocol for a randomized controlled trial. *Trials* 2019; 20:762.
 30. Lv ZT, Shen LL, Zhu B, et al. Effects of intensity of electroacupuncture on chronic pain in patients with knee osteoarthritis: a randomized controlled trial. *Arthritis Res Ther* 2019; 21:120.
 31. Feng PP, Deng P, Liu LH, et al. Electroacupuncture alleviates postoperative cognitive dysfunction in aged rats by inhibiting hippocampal neuroinflammation activated via microglia/TLRs pathway. *Evid Based Complement Alternat Med* 2017; 2017:6421260.
 32. Huang X, Huang K, Li Z, et al. Electroacupuncture improves cognitive deficits and insulin resistance in an OLETF rat model of Al/D-gal induced aging model via the PI3K/Akt signaling pathway. *Brain Res* 2020; 1740:146834.
 33. Wu J, Zhao Z, Sabirzhanov B, et al. Spinal cord injury causes brain inflammation associated with cognitive and affective changes: Role of cell cycle pathways. *J Neurosci* 2014; 34:110989-11006.
 34. Lu GF, Zhang JM, An JX, et al. Enhanced pain sensitivity with systemic ultrastructural changes of the nervous systems after cobra venom injection is reversed by electroacupuncture treatment. *Pain Physician* 2018; 21:E509-E521.
 35. Ji RR, Berta T, Nedergaard M. Glia and pain: Is chronic pain a gliopathy? *Pain* 2013; 154 Suppl 1:S10-S28.
 36. Basbaum AI, Bautista DM, Scherrer G, Julius D. Cellular and molecular mechanisms of pain. *Cell* 2009; 139:267-284.
 37. Tajerian M, Leu D, Zou Y, et al. Brain neuroplastic changes accompany anxiety and memory deficits in a model of complex regional pain syndrome. *Anesthesiology* 2014; 121:852-865.
 38. DeSouza DD, Hodaie M, Davis KD. Abnormal trigeminal nerve microstructure and brain white matter in idiopathic trigeminal neuralgia. *Pain* 2014; 155:37-44.
 39. Shiers S, Pradhan G, Mwirigi J, et al. Neuropathic pain creates an enduring prefrontal cortex dysfunction corrected by the Type II diabetic drug metformin but not by gabapentin. *J Neurosci* 2018; 38:7337-7750.
 40. Tanaka H, Homma H, Fujita K, et al. YAP-dependent necrosis occurs in early stages of Alzheimer's disease and regulates mouse model pathology. *Nat Commun* 2020; 11(1):507.
 41. McNamara RK, Hussain RJ, Simon EJ, et al. Effect of myristoylated alanine-rich C kinase substrate (MARCKS) overexpression on hippocampus-dependent learning and hippocampal synaptic plasticity in MARCKS transgenic mice. *Hippocampus* 2005; 15:675-683.
 42. Pinner AL, Haroutunian V, Meador-Woodruff JH. Alterations of the myristoylated, alanine-rich C kinase substrate (MARCKS) in prefrontal cortex in schizophrenia. *Schizophr Res* 2014; 154:36-41.
 43. Wang Y, Zeng C, Li J, et al. PAK2 Haploinsufficiency Results in synaptic cytoskeleton impairment and autism-related behavior. *Cell Rep* 2018; 24:2029-2041.
 44. Mao R, Deng R, Wei Y, et al. LIMK1 and LIMK2 regulate cortical development through affecting neural progenitor cell proliferation and migration. *Mol Brain* 2019; 12:67.
 45. Marlin JW, Chang YW, Ober M, Handy A, Xu W, Jakobi R. Functional PAK-2 knockout and replacement with a caspase cleavage-deficient mutant in mice reveals differential requirements of full-length PAK-2 and caspase-activated PAK-2p34. *Mamm Genome* 2011; 22:306-317.

Supplemental Table 1. *The detailed gene and protein information.*

Genes selected by the special screen rules in hippocampus			
Name	SHAM_H_ CV_H	SHAM_H_ EA_H	SHAM_H_ PRE_H
Prl	-4	1.247927513	#NUM!
Pak2	-3.793321794	-0.853833672	-3.381482468
Adam33	-3.321928095	-0.843880798	-1.881355504
LOC102555624	-3.169925001	-0.506959989	-0.754887502
LOC108352354	-2.906890596	-0.447458977	-1
LOC103694867	-2.660484851	-1.252226987	-1.649982293
Kcna3	-2.243454037	-1.045514659	-1.376720568
RGD1564247	-2.071603009	-0.123095923	-1.536855382
LOC100909849	-1.968237399	-0.761561436	-1.108385258
Cntnap5a	-1.6923268	-0.608057883	-0.945865736
LOC103692307	-1.688313385	-0.615221874	-1.931811971
LOC100910771	-1.619993606	-0.281799328	-1.2050643
Kcna2	-1.61074591	0.123979875	-1.098958668
LOC100911402	-1.55232666	-0.359604413	-0.734680299
Col8a1	-1.415037499	-0.263034406	-2.362570079
Ldlrad3	-1.362765553	-0.32363939	-1.540920253
LOC100911549	-1.320659632	0.140499913	-0.717398852
Igfbp2	-1.26608621	-0.18740286	-0.5526008
Elmod2	-1.163834174	0.121205383	-0.299447802
Hells	-1.15554212	0.047283243	-0.339860888
Nkx2-1	1.016405104	0.046998532	0.639831786
Sap25	1.069205471	-0.407033001	0.126269154
Catsperb	1.0704868	-0.127422402	0.617312951
LOC103692182	1.105273879	-0.166727423	0.257737676
LOC100911675	1.12042574	-0.072824368	0.357519928
Scn5a	1.140950825	-0.569855608	0.26934818
Ppp1r17	1.180572246	-0.263034406	0.30256277
LOC681458	1.23473299	0.174511289	0.377769941
LOC103692848	1.266786541	0.266786541	0.417852515
LOC103692173	1.355304232	0.119896215	0.598498461
LOC300308	1.391399171	0.20322085	0.723646177
LOC100910061	1.475142306	0.216444846	2.308356462
Ccdc24	1.490509078	0.290545969	0.557887553
LOC680885	1.504231229	0.362570079	0.893084796
Calcr	1.527247003	0	0.497499659
LOC100361018	1.561311233	0.549338591	1.06871275
RGD1563200	1.691877705	0.387023123	0.7589919
LOC102550026	1.750235238	0.399400393	0.914834285
Sgcg	1.898120386	0.628031223	0.937344392
LOC102550797	1.904174507	-0.160065678	0.72561467
RGD1561558	1.916744496	-1.261686722	1.277428635
Pura	1.991102893	0.800789514	1.046194746

Genes selected by the special screen rules in hippocampus			
Name	SHAM_H_ CV_H	SHAM_H_ EA_H	SHAM_H_ PRE_H
Atp6v1b1	2.113262425	0.705661204	2.276657526
Rps20	2.167450885	0.232624344	1.979966735
LOC100911537	2.223405194	-0.687830872	0.823474587
Acat1	2.288314478	0.199783349	2.549622795
LOC102552911	2.540568381	1.447458977	1.750021747
LOC108352957	2.887717606	0.833407189	2.199112014
LOC100911365	3.187273595	1.89648282	3.551990688
LOC103694169	3.566120426	1.998407579	4.464095352
LOC102555114	3.659924558	#NUM!	3.217230716
LOC108348139	3.696937813	-0.496412064	3.366396944
LOC102551071	3.946535348	1.314732593	3.169127271
Uap1l2	#NUM!	-0.123527505	-2.213521391
Rcor2	#NUM!	-0.464206421	-1.539494548
Impad1	#DIV/0!	#DIV/0!	#DIV/0!
Fastkd5	#DIV/0!	#DIV/0!	#DIV/0!

Genes selected by the special screen rules in PFC			
Name	SHAM-CV	SHAM-EA	SHAM-PGB
LOC100362965	-4.39053871	-1.73801292	-3.97385524
LOC100909844	-4.26884696	-1.1624249	-2.60116666
Pak2	-3.65300438	-0.36610729	-1.99845519
Fbxl8	-3.26145855	1.156725504	-0.62290407
Marcks	-3.22612432	-0.28592397	-2.54106955
LOC108352634	-2.8640663	-0.10195757	-2.91618903
LOC102547029	-2.45123587	-0.08893659	-1.6141715
LOC100911807	-2.40156299	0.321803127	-0.7828835
Potef	-2.3375868	-0.31468342	-0.82240822
Tm4sf19	-2.26303441	-0.4150375	-1.47560194
LOC102556148	-2.11625199	0.08053595	-1.56771586
Cyp4f5	-1.98646359	-0.58502268	-2.20488711
LOC108353410	-1.76553475	0.234465254	-0.83953533
Yod1	-1.73696559	0.047305715	-1.44745898
Fosl1	-1.73271612	-0.11973924	-0.73271612
Adat3	-1.71026695	-0.22314744	-0.65502352
Ecm2	-1.70882957	-0.14460459	-1.59557275
Ptger2	-1.6918777	-0.22239242	-0.18286406
Cntnap5a	-1.6876921	0.074283435	-0.89965065
Bend7	-1.66742466	-0.20029865	-1.05444778
LOC108353281	-1.66579784	0.182494656	-1.44711598
LOC501038	-1.66296501	0.498026864	-1.3734584
LOC103690102	-1.64475877	0.328990614	-1.48003764
RGD1564247	-1.63717856	0.172520304	-1.87925335

Supplemental Table 1 (cont.). *The detailed gene and protein information.*

Genes selected by the special screen rules in PFC			
Name	SHAM-CV	SHAM-EA	SHAM-PGB
Pim1	-1.62343665	-0.35715658	-0.66296501
Dusp4	-1.61218397	-0.43768624	1.557741032
Sik1	-1.60894136	-0.31797008	-3.25986713
LOC108352632	-1.60251539	0.471298385	-0.57826785
LOC100910270	-1.59509688	-0.09680744	-0.77917478
Htr5a	-1.59282462	0.482062593	-0.71620703
LOC103690017	-1.58433002	0.175969095	-1.18406996
LOC103690149	-1.58095724	0.108235529	-1.38532447
Htr1a	-1.56071495	0.094636874	-1.42321143
LOC102557368	-1.54136995	-0.33978257	-0.79890918
LOC100910771	-1.5357193	0.105547665	-1.36487333
LOC108353265	-1.52821927	0.110297409	-0.74089263
Kcna3	-1.50901365	0.856635825	3.06667104
LOC102553506	-1.50223511	0.188461329	-0.13111191
St8sia4	-1.49880586	-0.2410081	4.474485964
LOC100910056	-1.48294156	0.346332732	-0.68016808
Amph	-1.46893703	-0.13348869	-2.45640041
Fam98b	-1.45421479	0.389037871	-0.37327057
Cfap53	-1.45029043	0.008575485	-0.29232015
Slc6a11	-1.40399923	-0.27773546	-0.77855766
Rfxapl1	-1.39225198	0.028978069	-0.47106742
Chrb2	-1.36861316	0.285211197	-2.65632554
Gpd1l	-1.3515789	-0.10572751	-0.91891151
Htr1b	-1.3479233	-0.28379297	-0.96605267
LOC103691744	-1.33961037	0.856139747	-1.89495757
LOC100910838	-1.33664547	0.099170904	-0.64040082
LOC102556337	-1.32905343	-0.26957554	-1.05606905
Bhlha15	-1.3081223	-0.08572987	-0.37851162
Dgcr2	-1.29062915	0.401727432	-0.91674946
LOC100909476	-1.27872579	0.195489203	-0.84289698
Syt13	-1.26029944	0.207454301	-4.91237613
Htr2a	-1.25873427	0.334790246	1.223929656
Cdh5	-1.23798928	-0.0507448	-0.59162623
Maml3	-1.23562825	-0.16745675	-0.6662626
Exoc8	-1.23502003	-0.19849415	-3.25528545
LOC103693640	-1.23283051	0.059229912	-0.98808615
Slc1a4	-1.22633152	-0.06641192	-0.77381932
LOC102548151	-1.21089678	0.078609835	-0.29335894
Pcdhgc5	-1.20667412	0.655005217	-0.6612013
Chtop	-1.19683663	0.078668318	-0.80632909
Dhx33	-1.19417255	-0.02515348	-1.51436963
Atp6v0e2	-1.19242514	-0.14426836	-0.953042
Xylt1	-1.18937736	0.303490847	5.20438017

Genes selected by the special screen rules in PFC			
Name	SHAM-CV	SHAM-EA	SHAM-PGB
Hdx	-1.18903382	0.144389909	-1.51096192
Dck	-1.18737014	0.198413558	-1.17687776
LOC100911515	-1.18091947	-0.02289432	-0.5185113
Pcyox1	-1.17594879	0.198377737	-3.3326545
LOC100909679	-1.16583243	-0.06505529	-0.6248271
LOC103689975	-1.16298258	-0.0961775	-0.47453585
LOC100912076	-1.15257943	0.152045142	-0.69365779
Lifr	-1.14984821	-0.0460124	-3.4433479
Fat4	-1.14369877	-0.02749378	-0.53242752
Gabrb3	-1.1432737	0.458329062	-0.78629331
Ints9	-1.14239064	-0.06280681	2.409230714
Nt5dc3	-1.13047938	-0.09980904	-0.7079213
C11H22orf29	-1.12959925	-0.07681183	-0.49575057
LOC100910143	-1.12719595	0.214043489	-0.83400441
Nkrf	-1.12267166	0.318564147	-0.72176736
Kcnfl	-1.1064398	0.221862506	-0.85767197
Rab39a	-1.09621532	0.394531844	-1.1213063
Pcdhga7	-1.07789893	0.086476578	-6.26350165
Pcdhb3	-1.07662128	-0.02087873	-1.36516642
Bach2	-1.07594885	0.018378529	-0.76184026
Necab1	-1.07196979	0.240332902	-1.62229865
Eno2	-1.06745115	0.186572114	-0.45068389
Ankrd61	-1.05733318	0.733213459	-0.5943612
Ppm1e	-1.05532707	0.128384879	-0.84571326
Egr1	-1.05458449	0.194230841	-0.66870947
Sap25	0.982976145	-1.27589165	0.637812954
LOC108352957	0.992872009	-0.1909755	1.002895761
LOC103692936	1	-0.51739922	0.439532061
LOC103693723	1.014899844	-0.8236839	0.303651969
Lrrc71	1.03571909	-0.26383287	0.60396512
LOC103694046	1.038819249	-0.45943162	0.368387406
Defb1	1.087462841	-0.19264508	-1.5849625
Npff	1.08871063	0.077198886	3.973723841
Scube3	1.127661618	-0.20718618	4.087392987
LOC103693210	1.160593309	-0.50879431	0.497134679
LOC102550577	1.182983669	-0.19324328	0.444357577
RGD1561667	1.240131554	-0.48763335	4.681404011
Ak5	1.436712886	0.140631579	0.675859152
Fuom	1.505538874	-0.08483667	4.335651814
Draxin	1.51141248	0.196475047	1.096416692
Pura	1.523089733	-0.31861098	1.213721341
Atp6v1b1	1.565308196	-0.44489834	0.566458249
Dusp13	1.568184712	-0.03338973	1.360794454

Supplemental Table 1 (cont.). *The detailed gene and protein information.*

Genes selected by the special screen rules in PFC			
Name	SHAM-CV	SHAM-EA	SHAM-PGB
LOC100911685	1.711162736	-0.16192616	0.750393935
Oxt	1.736965594	0.152003093	2.223079255
Slc27a6	1.767553914	0.141914276	3.751967758
Lefty2	1.882139825	0.033740212	1.581990934
LOC108351576	1.901195731	0.059057556	1.133418579
LOC103690099	2.148651633	1.176628542	1.361465798
RGD1561185	2.236467607	-1.19129865	1.847647628
Pigr	2.420630687	1.013038	1.605303621
Sec14l3	2.951997266	1.289208415	-4.41418812

Supplemental Table 2. *Clean reads quality metrics.*

Sample	Total Raw Reads(M)	Total Clean Reads(M)	Total Clean Bases(Gb)	Clean Reads Q20(%)	Clean Reads Q30(%)	Clean Reads Ratio(%)
SHAM_C_1	70.85	66.78	6.68	97.78	90.54	94.25
SHAM_C_2	70.92	66.52	6.65	97.69	90.19	93.8
SHAM_C_3	70.81	66.2	6.62	97.69	90.33	93.49
SHAM_C_4	70.9	67.14	6.71	97.83	90.6	94.7
SHAM_C_5	68.47	65.16	6.52	97.84	90.67	95.18
SHAM_H_1	71.11	67.19	6.72	97.66	90.22	94.49
SHAM_H_2	68.82	65.29	6.53	97.73	90.56	94.88
SHAM_H_3	71.32	67.3	6.73	97.63	90.1	94.36
SHAM_H_4	68.88	65.36	6.54	97.8	90.48	94.9
SHAM_H_5	70.98	66.65	6.67	97.53	89.72	93.91
CV_C_1	68.53	65.27	6.53	98	91.28	95.24
CV_C_2	69.72	65.2	6.52	97.85	91.35	93.52
CV_C_3	68.57	65.61	6.56	97.92	91.12	95.68
CV_C_4	68.88	65.85	6.58	97.97	91.2	95.59
CV_C_5	68.65	65.32	6.53	97.9	91.07	95.16
CV_H_1	68.6	65.42	6.54	98.01	91.2	95.36
CV_H_2	68.53	65.14	6.51	97.93	90.96	95.06
CV_H_3	70.86	67.17	6.72	97.91	90.95	94.79
CV_H_4	70.82	66.86	6.69	97.71	90.29	94.4
CV_H_5	68.63	65.58	6.56	98.06	91.62	95.57
EA_C_1	69.47	66.37	6.64	97.84	90.69	95.54
EA_C_2	69.64	65.35	6.54	97.62	90.03	93.84
EA_C_3	69.65	65.65	6.57	97.66	90.2	94.26
EA_C_4	69.64	65.15	6.52	97.48	89.56	93.56
EA_C_5	69.64	65.52	6.55	97.53	89.72	94.08
EA_H_1	68.53	65.17	6.52	97.81	90.78	95.09
EA_H_2	71.18	67.23	6.72	97.63	90.18	94.45
EA_H_3	71.28	67.07	6.71	97.64	90.23	94.09
EA_H_4	68.83	65.04	6.5	97.71	90.44	94.49
EA_H_5	71.18	67	6.7	97.47	89.57	94.13
PGB_C_1	69.64	65.36	6.54	97.56	89.94	93.85
PGB_C_2	69.66	65.7	6.57	97.5	89.46	94.31
PGB_C_3	69.73	65.73	6.57	97.3	88.78	94.27
PGB_C_4	71.25	65.8	6.58	96.84	87.33	92.36
PGB_C_5	69.64	65.09	6.51	97.46	89.44	93.47
PGB_H_1	69.66	65.1	6.51	97.47	89.69	93.46
PGB_H_2	69.65	65.98	6.6	97.76	90.51	94.73
PGB_H_3	69.66	65.83	6.58	97.64	90.07	94.5
PGB_H_4	69.65	65.76	6.58	97.77	90.69	94.41
PGB_H_5	69.72	65.54	6.55	97.62	90.34	94

Supplemental Table 3. *Summary of genome mapping.*

Sample	Total CleanReads	Total MappingRatio	Uniquely MappingRatio
SHAM_C_1	66781380	0.9341	0.7117
SHAM_C_2	66521720	0.9327	0.7182
SHAM_C_3	66196748	0.9323	0.7216
SHAM_C_4	67140096	0.9402	0.7339
SHAM_C_5	65164114	0.9407	0.7281
SHAM_H_1	67186466	0.9391	0.7215
SHAM_H_2	65292936	0.9384	0.7308
SHAM_H_3	67302378	0.94	0.7399
SHAM_H_4	65364460	0.9397	0.7317
SHAM_H_5	66654964	0.9422	0.7469
CV_C_1	65,267,570	93.18%	71.14%
CV_C_2	65,202,784	89.42%	67.93%
CV_C_3	65,606,966	93.46%	69.43%
CV_C_4	65,848,130	93.19%	69.53%
CV_C_5	65,324,542	93.63%	72.13%
CV_H_1	65,416,184	93.79%	72.27%
CV_H_2	65,141,622	93.99%	73.36%
CV_H_3	67,166,674	93.96%	72.76%
CV_H_4	66,856,700	93.71%	72.59%
CV_H_5	65,583,848	93.34%	71.71%
EA_C_1	66,371,704	94.50%	73.25%
EA_C_2	65,354,062	91.99%	71.07%
EA_C_3	65,653,504	91.96%	71.48%
EA_C_4	65,153,960	92.15%	72.27%
EA_C_5	65,516,814	92.10%	71.92%
EA_H_1	65,166,110	94.19%	73.88%
EA_H_2	67,226,756	94.27%	73.99%
EA_H_3	67,070,868	94.28%	74.30%
EA_H_4	65,041,988	93.68%	72.97%
EA_H_5	66,995,554	94.49%	73.89%
PGB_C_1	65,357,438	91.45%	70.86%
PGB_C_2	65,697,528	91.76%	69.76%
PGB_C_3	65,731,522	92.48%	71.66%
PGB_C_4	65,804,732	92.97%	70.84%
PGB_C_5	65,091,082	91.33%	69.74%
PGB_H_1	65,104,236	92.01%	71.86%
PGB_H_2	65,982,072	92.42%	72.55%
PGB_H_3	65,828,418	92.52%	72.76%
PGB_H_4	65,758,860	91.91%	71.56%
PGB_H_5	65,543,514	91.70%	72.52%